J Mater Sci (2010) 45:5282–5290
DOI 10.1007/s10853-010-4572-7

Simultaneous monitoring of hydration kinetics, microstructural evolution, and surface interactions in hydrating gypsum plaster in the presence of additives

K. M. Song · J. Mitchell · H. Jaffel · L. F. Gladden

Received: 23 February 2010 / Accepted: 27 April 2010 / Published online: 14 May 2010

Abstract In this article, we use rapid two-dimensional nuclear magnetic resonance T_1–T_2 relaxation time correlations to monitor hydration kinetics, microstructural evolution, and surface interactions simultaneously in gypsum plaster pastes of industrial relevance. In particular, we explore the influence of ground gypsum mineral (GGM) as an accelerator and citric acid as a retarding agent in the hydration of the β form of plaster. Quantitative relative water fractions are determined and the modified hydration processes are observed as expected. These measurements also reveal the evolution of a secondary water population in the presence of the retarding agent when sedimentation of the hemihydrate occurs prior to crystallisation. In these samples, the ratio of relaxation times T_1/T_2 provides an indication of both the number and the strength of interactions between water molecules and solid gypsum particles. It is observed that the GGM decreases the T_1/T_2 ratio, whilst the citric acid increases the T_1/T_2 ratio, relative to the T_1/T_2 ratio in the unmodified plaster paste. We interpret this as an increase in the water–hemihydrate interaction in the presence of GGM, and a decrease in the presence of citric acid, consistent with the current understanding of the behaviour of these additives as an accelerator and retardant, respectively. The T_1 relaxation time measurements provide an indication of the pore structure evolution: larger pores are present in the accelerated product, and smaller pores in the retarded product, compared to the unmodified plaster. These conclusions are supported by helium porosimetry and scanning electron microscopy. The rapid T_1–T_2 measurement described here will be applicable to other reactions that evolve on a time scale of several minutes.

K. M. Song · J. Mitchell (✉) · L. F. Gladden
Department of Chemical Engineering and Biotechnology, University of Cambridge, Pembroke Street, Cambridge CB2 3RA, UK
e-mail: jm600@cam.ac.uk

H. Jaffel
Saint-Gobain Recherche, 39 Quai Lucien Lefranc, 93303 Aubervilliers, France

Introduction

The growth of calcium sulphate dihydrate ($CaSO_4 \cdot 2H_2O$ or gypsum) crystals is of considerable importance since it is encountered in a wide range of commercial applications, including the ceramics industry, as surgical and dental plaster, and as a building material. The macroscopic mechanical properties of gypsum-based plaster products are dependent on the structure of dihydrate crystals that form from the hemihydrate ($CaSO_4 \cdot 0.5H_2O$ or Plaster of Paris). It therefore follows that various production methods are required to control the structure, size, and morphology of these crystals. Both organic and inorganic additives can be included in plaster pastes to modify the hydration process. Additives generally alter the surface properties of the crystals which lead to changes in nucleation, growth, and hydration kinetics, resulting in variations in size and morphology as well as crystal habit [1]. In the plaster and cement industries, many additives are used as retarders or accelerators to control the growth of crystals and overall hydration kinetics. In general, it has been observed that strong inorganic acids, as well as salts of strong acids, and strong or weak bases are used as accelerators, whereas weak organic acids or their salts with strong bases act as retarders [1–4].

The influence of accelerators on the crystallisation of gypsum has been studied for many years [1–3, 5].

Accelerators include ground gypsum mineral (GGM), which is simply crushed dihydrate, and numerous neutral salts (e.g. sodium chloride, potassium chloride, and ammonium thiocyanate). It has been proposed that GGM acts as an accelerator by providing additional sites for nucleation (i.e. increasing the number of water–gypsum interactions), whereas salts modify the transport properties of ions and increase the dissolution rate of the hemihydrate [6]. Likewise, many studies have been carried out using carboxylic acids (adipic, malic, succinic, tartaric, and citric) as retarders of the crystallisation of gypsum, and as additives to improve the mechanical properties of set plaster [7–14]; although, it has been reported that tartaric acid, uniquely, provides almost no retardation of the hydration [11, 12]. Citric acid has been explained as providing a significant retarding effect because the acid molecules preferentially adsorb on the gypsum surfaces due to the similarity in distance between oxygen atoms in the acid and calcium atoms in the hemihydrate [13]. This preferential adsorption of the acid molecules reduces the number of active sites available for water–gypsum interactions.

Typically, the effects of additives have been studied by measuring the electrical conductivity through a suspension of hemihydrate [8, 10]. When the gypsum crystallisation begins, the conductivity drops; this sudden change in conductivity is closely related to physical and chemical changes in the sample [13]. Some authors have published results for industrially relevant plaster slurries, as studied here; see for example [15]. However, the electrical conductivity measurement is used most commonly for examining the growth of crystals in dilute suspensions [16, 17]. Another popular method of observing hydration kinetics is via temperature monitoring using techniques such as differential thermal analysis (DTA) [12, 15, 18]. Less common methods include acoustic transmission [13, 19], luminescence rigidochromism [20], and Fourier transform infra-red (FTIR) spectroscopy [12].

Studying the microstructural changes incurred by the use of additives requires a different set of techniques. The gypsum crystal structures that form during hydration are observed generally using microscopy techniques, such as optical microscopy [21, 22], scanning electron microscopy (SEM) [19, 23], and more recently, X-ray micro-computerised tomography (μ-CT) [24]. Many authors have used these techniques to observe the different gypsum crystal structures, and hence pore structures, that form in the presence of additives; a selection of the relevant literature is represented by the references herein including [3, 4, 25].

Nuclear magnetic resonance (NMR) offers a suite of non-destructive, in situ measurements that can be applied to investigate the setting of gypsum plaster in paste or slurry formulations. In previous works, the hydration of plaster pastes was monitored using NMR transverse relaxation time (T_2) measurements [5, 26]. The mobile water in the evolving pore structure is free to diffuse and exhibits long relaxation times on the order of, typically, $T_2 \approx 10\text{-}1000$ ms. In contrast, the water bound in the gypsum crystals has a very short $T_2 \approx 10\text{-}20$ μs. It is usual to observe only the mobile water fraction in these measurements. The degree of hydration can be determined by observing the signal intensity of the long T_2 components as a function of time: this decreases as the mobile water becomes bound in the crystal structure. Further to this, the evolution of the pores between the crystals can be monitored since the relaxation time is sensitive to the surface-to-volume ratio S/V of the heterogeneous solid [27]. Recently, we used both longitudinal (T_1) and transverse (T_2) relaxation time measurements to compare the hydration kinetics and pore structure in commercial α and β forms of plaster [24]. Elsewhere, the liquid-surface interactions in set plasters have been studied using field-cycling NMR [28]. In order to characterise the crystal or pore structures that form during hydration, it is necessary to combine these NMR techniques with results from optical analyses such as SEM and μ-CT [5, 24]. Information on the relationships between microscopic structure and macroscopic performance (e.g. strength, durability) can be obtained by including mechanical measurements [26].

The hydration kinetics of plaster pastes have been monitored previously using one-dimensional spin-echo profiles [24]. A basic spin-echo profile offers a measurement that contains, inherently, T_2 relaxation contrast ensuring the profile is only sensitive to mobile water in the plaster paste. Single point imaging (SPI) techniques [29, 30] can also be useful since they offer the ability to spatially resolve the bound water in cements and plasters [31, 32], although this is not required to monitor hydration kinetics.

In this article, we use a rapid two-dimensional T_1–T_2 relaxation correlation measurement to monitor simultaneously the hydration kinetics (from the quantitative signal amplitude of the mobile water), the evolution of the pore structure (from the separate longitudinal T_1 and transverse T_2 relaxation times), and to provide a qualitative description of the surface interactions (from the T_1/T_2 ratio). T_1–T_2 correlations [33] have become popular following the introduction of an efficient computational method of compressing the two-dimensional data into the form of a linear Fredholm integral [34] so that it can be inverted using standard Tikhonov regularisation. These type of data inversion problems (referred to incorrectly in much of the literature as "Laplace inversions") are ill-posed due to the infinite number of possible solutions; here, we use the generalised cross validation (GCV) [35] method to determine an optimum solution by minimising the difference between the fit error and the smoothing of the resultant

distribution. T_1–T_2 correlations have been applied previously to hydrating cement pastes [36, 37] where the acquisition time of each two-dimensional data set was on the order of 1 h. This was acceptable as the hydration processes being monitored in the cement occurred over several days. In the case of the plaster pastes studied here, the total hydration time can be less than 1 h [15], particularly in the presence of accelerants. Therefore, we use a modified data acquisition to allow multiple T_1–T_2 correlation plots to be obtained during the hydration process [38]. T_1/T_2 ratio measurements have been used previously to observe and compare strengths of surface interaction in cements [36] and oil reservoir rocks [39]. In such materials, the T_1/T_2 ratio is interpreted in terms of surface diffusion: ^{1}H nuclei in surface diffusing species encounter paramagnetic impurities and the frequency-dependent T_1/T_2 ratio is governed by proton–electron interactions [40]. However, when paramagnetic surface species are not present, the absolute value of the T_1/T_2 ratio is governed by both the strength of the adsorbate–adsorbent interactions and the total number of interactions. This was demonstrated by Liu et al. [41] in studies of porous silica glasses where it was observed that, in the case of strongly absorbing species, surface modifications influenced T_1 significantly more than T_2, resulting in a change in the T_1/T_2 ratio. This interpretation is applicable to previous T_1–T_2 studies of catalysts [42] and the gypsum-based materials in this work.

We apply rapid T_1–T_2 measurements to compare the hydration and microstructure in β plaster with GGM and citric acid as an accelerant and retardant, respectively. GGM, when added to hemihydrate, accelerates the hydration by providing additional nucleation sites for crystal growth [3]. In low concentrations (as used here), carboxylic acids are assumed to block access of water molecules to the active sites on the hemihydrate grains, slowing the onset of crystallisation [10–13]. Specifically, the formation of calcium citrate prevents water adsorption at dihydrate crystal boundaries [7]. In these earlier works, this hypothesis was supported by results from conductivity, pH, thermal, infra-red, and acoustic measurements that indicated adsorption (specifically, chemisorption) of the acid molecules onto the solid hemihydrate grains. For this reason, we are interested in monitoring not only the hydration kinetics and microstructural evolution, but also the water/gypsum interaction. These rapid T_1–T_2 measurements provide more information than their one-dimensional T_1 and T_2 counterparts without a significant increase in experimental time, as long as a sufficient signal-to-noise ratio can be obtained. Using the experimental method described here, which incorporates modifications demonstrated elsewhere [36, 38], T_1–T_2 correlations can be used to monitor in situ a range of reactions that occur on a time scale shorter than 1 h.

Materials and methods

All the plaster paste samples were made from commercial β plaster powder (purity >98 wt%). The pastes were prepared by manual mixing of the plaster powder with deionised water at a water-to-plaster ratio $w/p = 0.8$ by mass. Immediately after mixing, approximately 50 g of the pastes were introduced into 25 mm × 100 mm (diameter × height) glass tubes and sealed to prevent evaporation. For the accelerator studies, 0.1 wt% GGM was added to the dry hemihydrate. For the retarding agent studies, 0.1 wt% citric acid was added to the water prior to mixing with plaster powder. The same w/p was used in all the experiments.

All the NMR experiments were conducted on a 2 T horizontal imaging magnet, controlled via a Bruker AV spectrometer. The paste samples were positioned horizontally in the birdcage radio frequency (rf) coil tuned to 85 MHz for ^{1}H. Excitation pulse lengths of $t_{90} = 15$ μs and $t_{180} = 30$ μs corresponding to tip angles of 90° (P_{90}) and 180° (P_{180}) rf pulses, respectively, were typical. The T_1–T_2 correlation pulse sequence comprised a saturation recovery measurement to encode T_1 [43] followed by a Carr-Purcell Meiboom-Gill (CPMG) echo train to encode T_2 [44, 45]; the complete T_1–T_2 pulse sequence is shown in Fig. 1. Good saturation (where the spins are distributed incoherently in the x–y plane) was achieved using a comb of 32 × 90° rf pulses with variable separation and variable homospoil gradients (required to dephase coherent spins rapidly). The T_1 recovery interval was varied logarithmically between $t_A = \tau_1 = 10$ ms and 15 s in 16 steps. The intensity of the even echoes in the CPMG echo train were acquired; these echoes were generated with a logarithmically incremented echo spacing [36] such that the echo train had the form

$$P_{90} - \alpha^0\tau_2 - \left[P_{180} - \alpha^i\tau_2 - (\text{echo}) - \alpha^i\tau_2 - P_{180} - \alpha^i\tau_2 - (\text{echo}) - \alpha^{i+1}\tau_2 - \right]_n,$$

where $\tau_2 = 50$ μs, $\alpha = 1.2947$, and the index i was incremented from $0, \ldots, n$ where n is the number of even echoes. In this way, the intensities of 32 even echoes were acquired across a total acquisition time of $t_B = 2.64$ s. Two repeat scans were required to implement the phase cycle necessary to remove any baseline offset in the acquired data. This variable echo spacing CPMG measurement has been validated previously for use with cement-based materials [36]. Although there is likely to be some additional signal attenuation in the later echoes due to molecular self-diffusion through susceptibility-induced magnetic field gradients, comparisons between the variable echo time CPMG data and fixed echo time CPMG data were

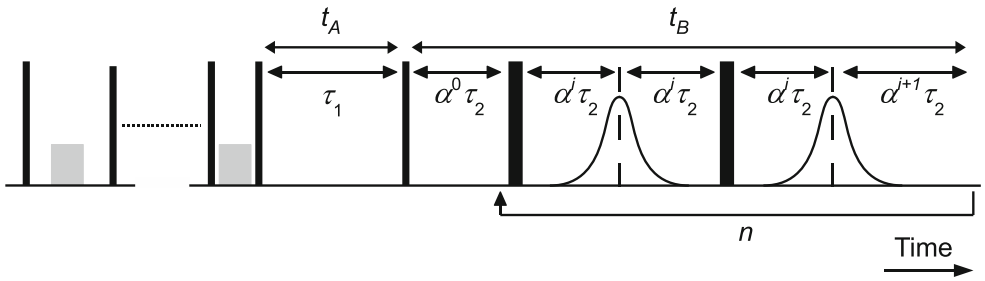

Fig. 1 The rapid T_1–T_2 relaxation correlation pulse sequence, employing saturation recovery followed by a CPMG echo train. The *thin* and *thick vertical lines* represent 90° and 180° rf pulses, respectively. The saturation recovery T_1 measurement consists of a comb of 90° pulses separated by variable delays and homospoil gradients (*grey rectangles*). Echo intensities were detected between alternate 180° rf pulses. The experimental timings are explained in detail in the text

seen to provide good agreement. Varying the echo time within the CPMG measurement offers the advantage of probing short relaxation time components without risk of spin-locking the system, and also reduces the rf duty cycle.

Saturation recovery was used to encode the T_1 dimension because it does not require a long recycle delay between successive acquisitions [38]. The recycle delay was $T_R = 100$ ms, providing a total acquisition time for a single two-dimensional 16 × 32 data set of 3 min. However, the saturation recovery sequence provides only half the dynamic range of the inversion recovery pulse sequence [43] utilised more commonly.

For the study of the gypsum crystal morphology, SEM images of the hydrated samples were acquired with a LEO 1530 and Supra VP Gemini scanning electron microscope utilising a field-emission gun at an acceleration voltage of 3 kV. The samples were prepared by pouring wet plaster pastes ($w/p = 0.8$) into 1.6 mm × 10 mm (diameter × height) sample tubes. These samples were allowed to hydrate for 1 h, and then dried overnight at 45 °C. For the helium porosimetry measurement, cylindrical hydrated and dried samples of dimensions 24 mm × 48 mm (diameter × height) were used to determine the pore volume with an ErgoTech (Conwy, UK) digital modular helium expansion volume meter. The grain volume was determined by helium expansion into a sealed sample cup, and the pore volume estimated by subtracting the grain volume from the total volume determined by measuring the external sample dimensions.

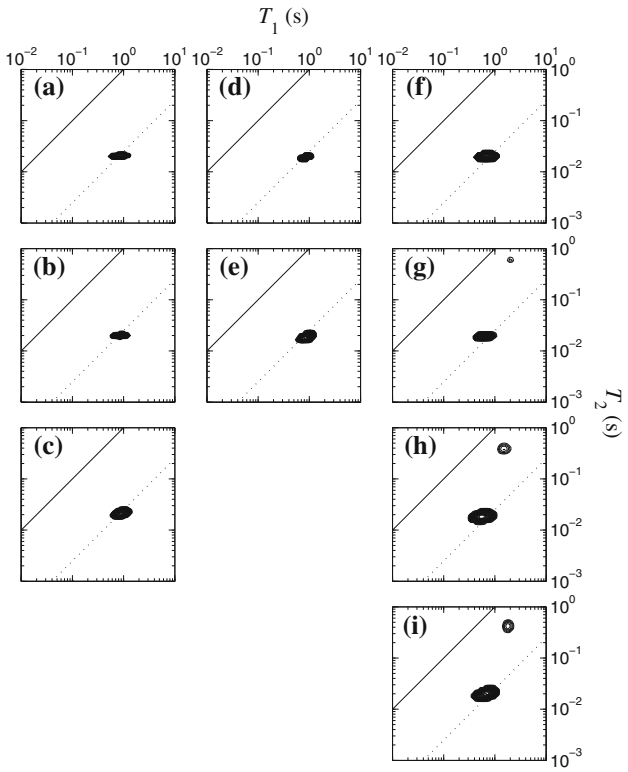

Fig. 2 T_1–T_2 correlation plots obtained for unmodified β plaster after **a** 3, **b** 20, and **c** 50 min of hydration. Equivalent plots are shown for β plaster with 0.1 wt% GGM after **d** 3 and **e** 20 min of hydration, and for β plaster with 0.1 wt% citric acid after **f** 3, **g** 20, **h** 50, and **i** 120 min of hydration. The contour intervals are the same in all plots. The *diagonal lines* indicate $T_1 = T_2$ (*solid*) and $T_1 = 40T_2$ (*dotted*)

Results and discussion

To monitor the hydration, both T_1 and T_2 relaxation times were observed simultaneously using rapid T_1–T_2 correlations. Example plots obtained for the unmodified β plaster, the β plaster with 0.1 wt% GGM, and the β plaster with 0.1 wt% citric acid are shown in Fig. 2. In the case of the unmodified β plaster, Fig. 2a–c, a single relaxation time component is observed for both T_1 and T_2, located at $T_1 \approx 40T_2$. The difference between the T_1 and T_2 values is due to the presence of the solid material resulting in liquid–solid surface interactions [46] and magnetic field gradients induced at the liquid–solid interfaces by magnetic susceptibility differences between the solid and liquid components [47]. As the hydration progresses there is little variation in the position of the peak, although the distribution broadens on the T_2 axis. This is indicative of an

evolution in the pore structure as has been discussed previously, where multiple discrete relaxation time components were detected in one-dimensional T_2 analyses of plaster pastes [5, 24, 26]. It was noted in these works that the majority of the signal (>90%) was associated with a single relaxation time. Additionally, it was shown that the broadening of one-dimensional T_2 distributions was consistent with the emergence of a long T_2 relaxation time component, corresponding to the evolution of large pores in β plaster [24]. Multiple T_2 relaxation times can be obtained from the T_1–T_2 data if required by fitting a discrete number of relaxation time components to the CPMG decays. The hydration process in the unmodified plaster reached completion at around 50 min hydration time.

The T_1–T_2 correlation plots for the β plaster paste with 0.1 wt% GGM, Fig. 2d, e are similar to the plots for the unmodified paste. Again, a single dominant relaxation time peak is observed. After 3 min of hydration this peak is located at $T_1 \approx 46T_2$, suggesting an increased interaction between the water and the gypsum particle surfaces in the presence of GGM when compared to the unmodified plaster. The hydration process was significantly faster in this modified paste, being complete after only 20 min, approximately. During the hydration process, the single relaxation time peak broadens slightly in both the T_1 and the T_2 dimensions, indicative of the evolution of the porosity. The increase in the peak area is similar to that observed for the unmodified plaster, albeit over a shorter time scale, suggesting the final pore size distributions do not differ significantly.

The T_1–T_2 correlation plots for the β plaster paste with 0.1 wt% citric acid, Fig. 2f–i, are notably different to the plots for the unmodified paste. Initially (after 3 min of hydration), the plaster paste with the citric acid additive exhibits a single dominant relaxation time component with $T_1 \approx 32T_2$ (further discussions of the T_1/T_2 ratio are given below). This component broadens on both the T_1 and the T_2 axes over the total hydration time, indicative of a broad distribution of pore sizes. As the initiation period progresses, the evolution of a second relaxation time peak is observed close to the $T_1 = T_2$ line. This is indicative of bulk water present in the sample. This is observed visually, where the hydrated β plaster paste with additive is seen to exhibit a layer of water on top of the solid material; this behaviour is not observed in the unmodified plaster. The emergence of the bulk water is attributed to sedimentation of the hemihydrate solids prior to crystallisation. This occurs in the presence of citric acid due to the increase in duration of the initiation period.

Information on the hydration kinetics has been obtained from the T_1–T_2 plots. Although these measurements are only sensitive to the mobile water content of the pastes, the integral of the peaks in the two-dimensional distributions provides a signal intensity that is independent of relaxation weighting and therefore directly proportional to the absolute volume of mobile water. It is also possible to distinguish water volumes in different physical environments. The relative amount of mobile water in the β plaster pastes is shown in Fig. 3. Over the total hydration time, the signal intensity is seen to decrease in all three pastes as a fraction of the mobile water combines with the gypsum hemihydrate to form dihydrate crystals. Three principle stages for the setting of plaster are observed. The initiation period occurs prior to the formation of gypsum crystals, and is related to the dissolution of hemihydrate and heterogeneous crystal nucleation [10, 15, 24]. The observed signal is approximately constant throughout the initiation period. Crystallisation occurs primarily during the acceleration period, defined by a notable decrease in the signal intensity as a fraction of the mobile water becomes bound into the gypsum crystals. The signal is again constant during the completion period after the crystallisation and precipitation processes have occurred. For the unmodified β plaster paste, Fig. 3 (open circle), the relative water volume decreases from 1.0 to 0.78 in agreement with the calculated stoichiometric value (relative water fraction) of 0.23 required to hydrate the hemihydrate completely [26]. The initiation (0–15 min), acceleration (15–27 min), and completion periods (>27 min) are observed as expected [24]; these times are comparable to hydration kinetics published elsewhere for β plaster [15]. When 0.1 wt% GGM is added

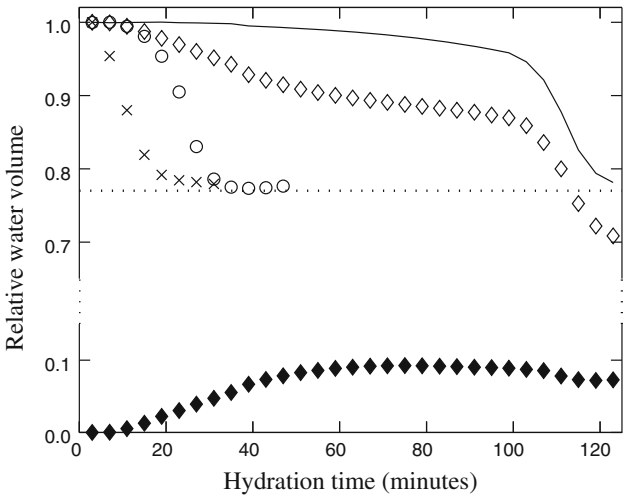

Fig. 3 Signal intensities extracted by integration of peaks in the T_1–T_2 correlation plots acquired during the hydration of plaster pastes. A single component is observed for the unmodified β plaster paste (*open circle*) and β plaster paste with 0.1 wt% GGM (*cross*), whereas two components are observed for the β plaster paste with 0.1 wt% citric acid: the primary water (paste) population (*open diamond*) and the secondary (bulk water) population (*filled diamond*); the *solid line* indicates the sum of these two components. The *horizontal dotted line* indicates the stoichiometric water fraction

to the β plaster paste (cross), the initiation period (<3 min) is not observed; only the acceleration (3–19 min) and completion periods (>19 min) are visible. The final relative water volume is 0.77, consistent with the unmodified hydrated plaster and the stoichiometric value.

The relative water volumes for the two populations present when the citric acid retarding agent is added are also shown in Fig. 3. Initially, all the mobile water is present in the paste (referred to here as the primary water population), comparable to the unmodified β plaster. However, as the initiation period progresses, the primary water population (open diamond) decreases, whilst a secondary water population (filled diamond), associated with bulk water, increases. This process occurs over the first 40 min of the total hydration time. For the next 60 min, the two water populations remain relatively constant in volume until crystallisation occurs at 100 min. At this stage, the primary water population decreases in volume rapidly. The total water volume in the sample (solid line) is obtained by summing the volumes of the two populations. As expected, the addition of citric acid results in an increase in the duration of the initiation period since the weak acid acts as an inhibitor for the dissolution processes by preventing access of water to the active surface sites on the hemihydrate crystals [8, 10, 13]. Over the entire initiation period (<100 min) there is only a slight loss in mobile water volume, likely due to some early stage crystal nucleation and growth. The final total water volume is almost identical to that observed for the unmodified β plaster, consistent with the same relative volume of water required to convert hemihydrate to gypsum despite the presence of citric acid.

The mean T_1 relaxation times for the water populations identified in Fig. 3 are shown in Fig. 4a. In the case of the unmodified plaster (open circle), the T_1 relaxation time shows a slight increase during the acceleration period (from T_1 = 0.85 to 0.96 s), consistent with the evolution of the pore structure (i.e. the formation of larger pores). The T_1 data are consistent with those published previously using rapid one-dimensional T_1 measurements [24]. In the presence of GGM, similar T_1 behaviour is observed, albeit on a shorter time scale. Here, the mean relaxation time increases from T_1 = 0.89 to 1.02 s over the acceleration period. The mean T_1 times are consistently longer than those observed in the unmodified paste, suggesting the rapid hydration results in larger pores and a less dense product.

For the β plaster with citric acid, two T_1 components are observed. Figure 4(a, open diamond) corresponds to the primary water population. For this water population, the T_1 relaxation time exhibits a slight decrease over the first 40 min (from T_1 = 0.69 to 0.59 s) and then remains almost constant until crystallisation occurs $\sim$100 min, at which point the T_1 relaxation time increases to T_1 = 0.77 s, consistent with the increase in T_1 observed in the unmodified

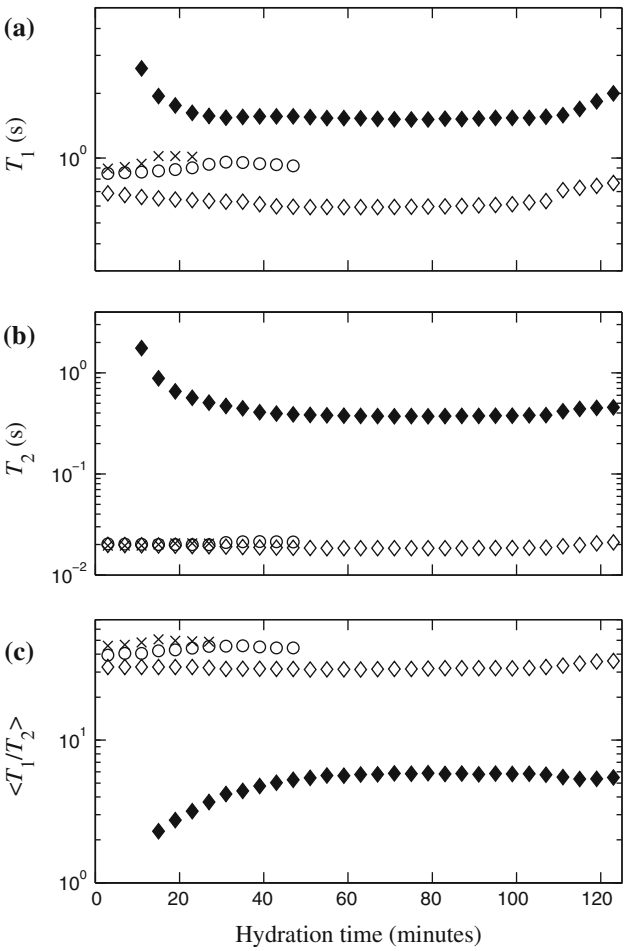

Fig. 4 Mean relaxation times extracted from T_1–T_2 correlation plots for the unmodified β plaster paste (*open circle*), β plaster paste with 0.1 wt% GGM (*cross*) and the two components in the β plaster paste with 0.1 wt% citric acid (*open diamond* and *filled diamond*), showing **a** T_1, **b** T_2, and **c** $\langle T_1/T_2 \rangle$. The *symbols* correspond with those in Fig. 3

plaster during the acceleration period. However, the T_1 in the modified paste is consistently shorter than the T_1 times for the unmodified plaster, suggesting smaller pores (and hence a denser structure) are formed. This is consistent with sedimentation of the solids during the initiation period.

The T_1 of the bulk water component in the presence of citric acid, Fig. 4(a, filled diamond), decreases initially (from T_1 = 2.61 to 1.55 s) and then remains constant until crystallisation occurs. This is consistent with the dissolution of soluble paramagnetic species leaching out of the plaster paste during the initiation period and altering the relaxation properties of the spins in the free-diffusing water molecules. During the acceleration period, the T_1 of this bulk water population increases to T_1 = 1.99 s.

The mean T_2 relaxation times for the plasters are shown in Fig. 4b. For the unmodified plaster (open circle) the T_2 relaxation time exhibits a slight increase in T_2 (akin to that

observed for T_1) over the acceleration period (from T_2 = 0.019 to 0.021 s). As noted above, this is accompanied by a broadening of the T_2 distribution, consistent with the evolution of the pore structure [24]. The T_2 behaviour of the plaster paste with GGM (b, cross) is almost indistinguishable from the unmodified plaster, except the observed increase in T_2 occurs on a shorter time scale consistent with the accelerated hydration. The mean T_2 times for the plaster paste with citric acid, Fig. 4(b, open diamond), are also equivalent to the T_2 relaxation times observed in the unmodified plaster.

The T_2 relaxation time of the excess water in the presence of citric acid, Fig. 4(b, filled diamond), decreases initially (from T_2 = 1.75 to 0.37 s) and then remains almost constant until gypsum crystallisation occurs, at which point a slight increase in T_2 is observed, to T_2 = 0.455 s. This is consistent with the T_1 behaviour of this water population.

It is significant that T_1 changes between the different paste compositions, whereas T_2 is almost invariant. T_1 is known to be more sensitive to the number of adsorbate–adsorbent interactions [41], whilst T_2 is governed predominantly by local variations of surface geometry and chemistry. It is also reasonable to expect T_1 to be more sensitive to variations in pore size since the T_1 measurement is sensitive to a longer time scale than T_2, allowing water molecules to explore more of the pore network.

The average ratio of relaxation times $\langle T_1/T_2 \rangle$ for the water populations identified in Fig. 3 are shown in Fig. 4c. In the unmodified plaster (open circle), the initial $\langle T_1/T_2 \rangle = 40$. In the presence of GGM (cross), the initial $\langle T_1/T_2 \rangle = 46$, and in the presence of citric acid (open diamond), the initial $\langle T_1/T_2 \rangle = 32$. These values are consistent with the expected variation in the number of active surface sites available for water adsorption in the different plasters: the addition of GGM increases the number of active sites, whilst the citric acid adsorbs preferentially, blocking access of the water molecules. This is in agreement with previous explanations of the citric acid preventing access of the water to active surface sites on the hemihydrate solids due to preferential adsorption [10–13].

As crystallisation occurs during the acceleration period, the $\langle T_1/T_2 \rangle$ ratio is seen to increase in all three samples due to the variation in T_1. For the unmodified plaster paste, Fig. 4(c, open circle), $\langle T_1/T_2 \rangle$ increases from 40 to 45; in the presence of GGM (cross) $\langle T_1/T_2 \rangle$ increases from 46 to 51; and in the presence of citric acid $\langle T_1/T_2 \rangle$ of the primary water population (open diamond) increases from 32 to 38. This consistent increase in the $\langle T_1/T_2 \rangle$ ratio (governed by T_1 variations) as the dihydrate is produced suggests that the dihydrate crystals have more active surface sites than the hemihydrate particles. This increased liquid–solid interaction has been observed previously by acoustic emission measurements [13].

An alternative interpretation of the $\langle T_1/T_2 \rangle$ ratios is a variation in the specific surface area S_p of the solid particles since T_1 is more sensitive to S_p than T_2. It has been shown elsewhere that low-field relaxation measurements can probe such changes in S_p of cement-based materials [48]. Using this interpretation, the difference in $\langle T_1/T_2 \rangle$ between the unmodified β plaster and modified plasters would suggest that the smallest crystals are formed in the presence of GGM and the largest crystals in the presence of citric acid; this correlation is confirmed by the SEM images in Fig. 5. However, the initial differences in $\langle T_1/T_2 \rangle$ and T_1 between the unmodified plaster and modified plasters is difficult to rationalise using this argument; whilst, the addition of GGM could lead to an initial increase in S_p, the gypsum hemihydrate particle size is identical, initially, between the unmodified plaster and in the presence of citric acid. Additionally, we do not expect the relaxation data to be particularly sensitive to changes in S_p at the resonant frequency of these measurements (f_0 = 85 MHz). Notwithstanding, it is worth acknowledging that changes in S_p could influence the results by varying the number of active sites available for adsorption, and hence lead to a change in T_1.

The $\langle T_1/T_2 \rangle$ ratio for the secondary water population in the plaster paste with citric acid, Fig. 4(c, filled diamond) is initially $\langle T_1/T_2 \rangle \approx 2$ (consistent with the assignment of this population to bulk water) but increases as the volume of bulk water increases (15–40 min total hydration time), again likely due to the influence of soluble paramagnetic chemical species leaching into the water as dissolution of the hemihydrate occurs.

The T_1–T_2 relaxation measurements indicate a difference in the hydration dynamics and pore structure evolution (influenced by the crystal habit) of the β plaster in the presence of additives. The crystal structures that form on hydration have been visualised with SEM imaging, see Fig. 5. In the unmodified plaster, Fig. 5a, needle-shaped gypsum crystals with a high degree of entanglement are observed. In the presence of GGM, Fig. 5b, similar crystal shapes are observed, although they tend to be thinner and shorter than in the unmodified plaster as a result of the rapid crystallisation. However, the citric acid modifies the morphology of the resultant gypsum crystals significantly, leading to the formation of large prismatic crystals in agreement with previous studies [6, 13]. From the SEM images, it is expected that the porosity of the hydrated sample with citric acid will be lower than in the unmodified sample as noted elsewhere [6]; the porosities of these hardened gypsum samples, determined by helium porosimetry, were found to be 57.9 ± 0.1% for the unmodified plaster, 58.2 ± 0.1% in the presence of GGM, and 55.3 ± 0.1% in the presence of citric acid. These results confirm the higher porosity of the accelerated product, and lower

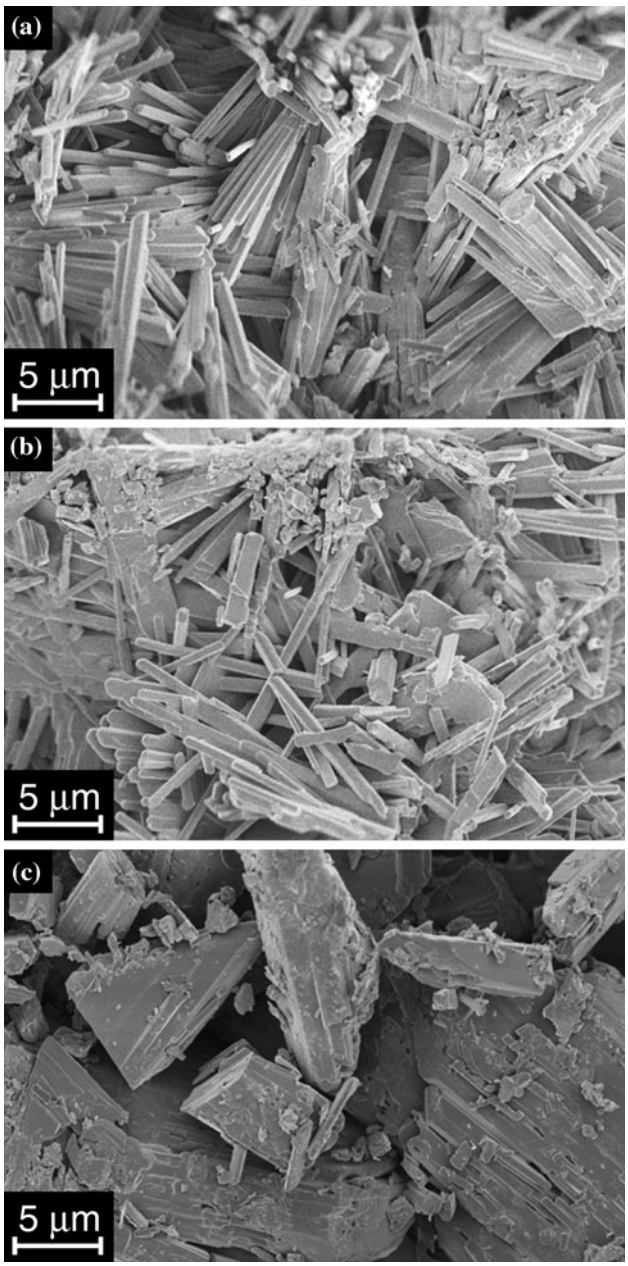

Fig. 5 SEM images of hydrated **a** unmodified β plaster, **b** β plaster with 0.1 wt% GGM, and **c** β plaster with 0.1 wt% citric acid

porosity for the retarded product, as implied by the mean T_1 values extracted from the T_1–T_2 correlations.

Conclusions

In this article, we have presented, for the first time, a rapid T_1–T_2 NMR relaxation time correlation experiment capable of probing simultaneously hydration kinetics, microstructural evolution, and water–gypsum interactions in plaster pastes. The addition of GGM resulted in a rapid hydration process, predominantly characterised by the absence of an initiation period on the time resolution of these measurements. The relaxation times observed were similar to those for the unmodified plaster, and this was reflected in the similar crystal morphology observed in the set products. The addition of citric acid as a retarding agent lead to an increase in duration of the initiation period of the hydration process. These data are consistent with previous conclusions that carboxylic acids are chemisorbed at the surface of hemihydrate grains during the initiation period, inhibiting the access of water to active surface sites and slowing the dissolution process [10–13]. This interpretation was supported by the different $\langle T_1/T_2 \rangle$ ratios, governed by changes in T_1, observed in the β plaster with and without additives.

The qualitative T_1–T_2 correlations revealed that the total water volume required to convert the hemihydrate to gypsum remained the same whether the additives were present or not. However, the gypsum crystal structures that formed were modified significantly by citric acid, as observed by SEM. The presence of bulk water was attributed to sedimentation of the hemihydrate solids prior to crystallisation as a result of the retarding action of the citric acid. In unmodified plasters, dissolution and sedimentation are thought to occur simultaneously with nucleation and crystallisation, providing a more homogeneous product [6].

The rapid T_1–T_2 correlation measurement utilised here will enable other time-sensitive systems to be studied in a similar manner. The inclusion of two dimensions allows signal intensities to be extracted that are more directly proportional to water volume than can be obtained easily from one-dimensional NMR measurements, and also provides an alternative manner of characterising the behaviour of liquids in different physical environments. The simple determination of relative liquid–solid surface interactions from these T_1–T_2 data sets provides additional information on the molecular dynamics that cannot be obtained so readily by other standard techniques. In future work, we will apply this experimental method to other plaster products to yield further understanding of the pore structure evolution when additives are present.

Acknowledgements The authors thank Mr. Thusara Chandrasekera for providing modifications to the inversion methods. K. M. Song thanks Dr J. Sohn of Cambridge Nanoscience Centre for assistance with the SEM and Mr J. Staniland of Schlumberger Cambridge Research for the helium porosimetry measurements. For financial support K. M. Song thanks Saint-Gobain and J. Mitchell thanks Schlumberger Cambridge Research.

References

1. Ridge MJ (1960) Rev Pure Appl Chem 10:243
2. Ridge MJ, Beretka J (1969) Rev Pure Appl Chem 19:17

3. Lewry AJ, Williamson J (1994) J Mater Sci 29:6085. doi: 10.1007/BF00354546
4. Panpa W, Jinawath S (2006) Adv Cem Res 18:145
5. Jaffel H, Korb JP, Ndobo-Epoy JP, Morin V, Guicquero JP (2006) J Phys Chem B 110:7385
6. Singh NB, Middendorf B (2007) Prog Cryst Growth Charact Mater 53:57
7. Koslowski T, Ludwig U (1984) The chemistry and technology of gypsum, ASTM STP, vol 861. American Society for Testing Materials, chap. Retardation of gypsum plasters with citric acid: mechanisms and properties, pp 97–104
8. Amathieu L, Boistelle R (1986) J Cryst Growth 79:169
9. Singh M, Garg M (1997) Cem Concr Res 27:947
10. Badens E, Veesler S, Boistelle R (1999) J Cryst Growth 198:704
11. Singh NB, Vellmer C, Middendorf B (2005) Indian J Eng Mater Sci 12:337
12. Vellmer C, Middendorf B, Singh NB (2006) J Therm Anal Calorim 86:721
13. Ersen A, Smith A, Chotard T (2006) J Mater Sci 41:7210. doi: 10.1007/s10853-006-0918
14. Magallanes-Rivera RX, Escalante-García JI, Gorokhovsky A (2009) Constr Build Mater 23:1298
15. Lewry AJ, Williamson J (1994) J Mater Sci 29:5279. doi: 10.1007/BF01171536
16. Galtier P, Soustelle M, Guilho B (1983) Cem Concr Res 13:703
17. Ludwig U, Singh NB (1978) Cem Concr Res 8:291
18. Bensted J, Varma SP (1972) Cem Technol 3:67
19. Lewry AJ, Williamson J (1994) J Mater Sci 29:5524. doi: 10.1007/BF003499
20. Kunkely H, Vogler A (2008) Mater Chem Phys 109:506
21. Miyazaki H (1968) Shinku Kagaku 15:113
22. Šatava V (1970) Sprechsaal Keram Glas Email 103:792
23. Kuzel HJ, Hauner M (1987) Zement-Kalk-Gips 40:628
24. Song KM, Mitchell J, Gladden LF (2009) J Mater Sci 44:5004. doi: 10.1007/s10853-009-3765
25. Witkamp GJ, van der Eerden JP, van Rosmalen GM (1990) J Cryst Growth 102:281
26. Jaffel H, Korb JP, Ndobo-Epoy JP, Guicquero JP, Morin V (2006) J Phys Chem B 110:18401
27. Brownstein KR, Tarr CE (1979) Phys Rev A 19:2446
28. Korb JP, Levitz PE (2009) AIP Conf Proc 1081:55
29. Emid S, Creyghton JHN (1985) Physica B & C 128:81
30. Balcom BJ, MacGregor RP, Beyea SD, Green DP, Armstrong RL, Bremner TW (1996) J Magn Reson A 123:131
31. Mastikhin IV, Mullally H, MacMillan B, Balcom BJ (2002) J Magn Reson 156:122
32. Faure P, Caré S, Po C, Rodts S (2005) Magn Reson Imaging 23:311
33. Song YQ, Venkataramanan L, Hürlimann MD, Flaum M, Frulla P, Straley C (2002) J Magn Reson 154:261
34. Venkataramanan L, Song YQ, Hürlimann MD (2002) IEEE Trans Signal Process 50:1017
35. Wahba G (1977) SIAM J Numer Anal 14:651
36. McDonald PJ, Korb JP, Mitchell J, Monteilhet L (2005) Phys Rev E 72:011409
37. McDonald PJ, Mitchell J, Mulheron M, Aptaker PS, Korb JP, Monteilhet L (2007) Cem Concr Res 37:303
38. Seland JG, Bruvold M, Brurok H, Jynge P, Krane J (2007) Magn Reson Med 58:674
39. Mitchell J, Hürlimann MD, Fordham EJ (2009) J Magn Reson 200:198
40. Kleinberg RL, Kenyon WE, Mitra PP (1994) J Magn Reson A 108:206
41. Liu G, Li Y, Jonas J (1991) J Chem Phys 95:6892
42. Weber D, Mitchell J, McGregor J, Gladden LF (2009) J Phys Chem C 113:6610
43. Vold R, Waugh J, Klein M, Phelps D (1968) J Chem Phys 48:3831
44. Carr H, Purcell E (1954) Phys Rev 94:630
45. Meiboom S, Gill D (1958) Rev Sci Instrum 29:688
46. Godefroy S, Korb JP, Fleury M, Bryant RG (2001) Phys Rev E 64:021605
47. Hürlimann MD (1998) J Magn Reson 131:232
48. Barberon F, Korb JP, Petit D, Morin V, Bermejo E (2003) Phys Rev Lett 90:116103